Author Manuscript Published OnlineFirst on March 29, 2016; DOI: 10.1158/0008-5472.CAN-15-1939
Author manuscripts have been peer reviewed and accepted for publication but have not yet been edited.

p53 loss in Myc-driven neuroblastoma leads to metabolic adaptations supporting radioresistance

Orli Yogev[1], Karen Barker[1], Arti Sikka[2], Gilberto S. Almeida[1,3], Albert Hallsworth[1], Laura M. Smith[1], Yann Jamin[3], Ruth Ruddle[4], Alexander Koers[1], Hannah T. Webber[1], Florence I. Raynaud[4], Sergey Popov[4,5], Chris Jones[4,5], Kevin Petrie[1,‡], Simon P. Robinson[3], Hector C. Keun[2] and Louis Chesler[1]

[1]Division of Clinical Studies, The Institute of Cancer Research, London, SW7 3RP, UK
[2]Department of Surgery and Cancer, Imperial College, London, SW7 2AZ, UK
[3]Division of Radiotherapy and Imaging, The Institute of Cancer Research, London, SW7 3RP, UK
[4]Division of Cancer Therapeutics, The Institute of Cancer Research, London, SW7 3RP, UK
[5]Department of Molecular Pathology, The Institute of Cancer Research, London, SW7 3RP, UK

Corresponding author: Louis Chesler, Pediatric Solid Tumour Biology and Therapeutics Team, Division of Clinical Studies, The Institute of Cancer Research, London, SW7 3RP, UK. Tel: +44 20 8722 4204, Fax: +44 208 7224134, e-mail: louis.chesler@icr.ac.uk.

Running title: Metabolic adaptation in high-risk neuroblastoma lacking p53.

Disclosure of Potential Conflicts of Interest: No potential conflicts of interest were disclosed.

[‡] Current address: School of Natural Sciences, University of Stirling, Stirling, FK9 4LA, UK.

Author Manuscript Published OnlineFirst on March 29, 2016; DOI: 10.1158/0008-5472.CAN-15-1939
Author manuscripts have been peer reviewed and accepted for publication but have not yet been edited.

Abstract

Neuroblastoma is the most common childhood extra-cranial solid tumor. In high-risk cases, many of which are characterized by amplification of MYCN, outcome remains poor. Mutations in the p53 (TP53) tumor suppressor are rare at diagnosis, but evidence suggests that p53 function is often impaired in relapsed, treatment-resistant disease. To address the role of p53 loss-of-function in the development and pathogenesis of high-risk neuroblastoma, we generated a MYCN-driven genetically engineered mouse model in which the tamoxifen-inducible p53ERTAM fusion protein was expressed from a knock-in allele (Th-MYCN/Trp53KI). We observed no significant differences in tumor-free survival between Th-MYCN mice heterozygous for Trp53KI (n=188) and Th-MYCN mice with wild-type p53 (n=101). Conversely, the survival of Th-MYCN/Trp53KI/KI mice lacking functional p53 (n=60) was greatly reduced. We found that Th-MYCN/Trp53KI/KI tumors were resistant to ionizing radiation (IR), as expected. However, restoration of functional p53ERTAM reinstated sensitivity to IR in only 50% of Th-MYCN/Trp53KI/KI tumors, indicating the acquisition of additional resistance mechanisms. Gene expression and metabolic analyses indicated that the principal acquired mechanism of resistance to IR in the absence of functional p53 was metabolic adaptation in response to chronic oxidative stress. Tumors exhibited increased antioxidant metabolites and upregulation of glutathione S-transferase pathway genes, including GSTP1 and GSTZ1, which are associated with poor outcome in human neuroblastoma. Accordingly, glutathione depletion by buthionine sulfoximine together with restoration of p53 activity re-sensitized tumors to IR. Our findings highlight the complex pathways operating in relapsed neuroblastomas and the need for combination therapies that target the diverse resistance mechanisms at play.

Author Manuscript Published OnlineFirst on March 29, 2016; DOI: 10.1158/0008-5472.CAN-15-1939
Author manuscripts have been peer reviewed and accepted for publication but have not yet been edited.

Introduction

p53 is a critical tumor suppressor that performs a diverse range of functions including induction of apoptosis, senescence and DNA repair in response to genotoxic stress. Deregulation of its activity is associated with tumor initiation and progression as well as resistance to therapy. Recent *in vivo* evidence indicates that the role of p53 as a tumor suppressor is independent of its canonical role as a cell cycle, senescence and pro-apoptosis regulator, and may be due to other p53-dependent activities such as maintenance of DNA stability and metabolic adaptation (1). In the last decade, a role for p53 in metabolic adaptation has been identified (2,3), often activated by metabolic stress induced by low oxygen levels or nutrient scarcity (3). This leads to changes in several metabolic mechanisms affecting energy homeostasis such as glycolysis, down-regulation of reactive oxygen species (ROS), oxidative phosphorylation (OXPHOS), β-oxidation and gluconeogenesis (4). However, to date there is no direct evidence demonstrating an advantage in tumor survival or growth *in vivo* due to metabolic alterations induced by p53 loss-of-function.

Neuroblastoma is the most common extracranial pediatric solid tumor and amplification of the *MYCN* gene is a predictor of high-risk disease. Treatment options for high-risk patients include intensive cytotoxic chemotherapy and surgical resection, myeloablative autologous stem cell transplantation, radiotherapy, and intensive multimodal therapy. Although most high-risk patients initially respond to therapy, a majority of these patients will relapse with treatment-resistant disease. Approximately 50% of relapsed tumors are associated with p53 loss-of-function, mainly through alterations to the p53 pathway. In contrast to other MYC-driven cancers, such as medulloblastoma (5) and lymphoma, mutation of genes in the p53 pathway is rare at diagnosis (6), implying that selection for p53 pathway deficiency occurs following treatment. Additional mechanisms such as epigenetic alterations and metabolic adaptation have also been implicated in aggressive neuroblastoma (7-11). To better understand the role of p53 in the development of high-risk therapy-resistant neuroblastoma, we generated a MYCN-driven genetically engineered mouse (GEM) model with inducible p53 loss-of-function.

Author Manuscript Published OnlineFirst on March 29, 2016; DOI: 10.1158/0008-5472.CAN-15-1939
Author manuscripts have been peer reviewed and accepted for publication but have not yet been edited.

Materials and Methods

In vivo studies

All experimental protocols were monitored and approved by The Institute of Cancer Research Animal Welfare and Ethical Review Body, in compliance with the UK Home Office Animals (Scientific Procedures) Act 1986, the United Kingdom National Cancer Research Institute guidelines for the welfare of animals in cancer research (12), and the ARRIVE guidelines (13). Th-*MYCN* mice (129X1/SvJ-Tg(Th-MYCN)41Waw/Nci) have been described previously (14). The $Trp53^{KI/KI}$ mice were kindly provided by G.I. Evan (15) and crossed with Th-*MYCN* animals into a background of the 129X1/SvJ-Tg(TH-MYCN)41Waw/Nci (for more than 15 generations). Transgenic Th-*MYCN*/$Trp53^{KI}$ animals with palpable tumor were allocated to treatment or control groups. Restoration of wild-type p53 was achieved by administration of chow containing tamoxifen at 400 mg/kg to provide a daily dose of approximately 64 mg/kg. Animals were monitored twice a week by palpation for detectable tumors (>5 mm) and were sacrificed upon detection of a tumor larger than 15mm diameter. Mice were allowed access to sterilized food and water *ad libitum*.

In vivo imaging

Multi-slice ^{1}H MRI was performed on a 7T horizontal bore microimaging system (Bruker Instruments) using a 3 cm birdcage coil. Anesthesia was induced using a gaseous mixture of 2% isoflurane/oxygen (v/v). Core body temperature was maintained by warm air blown through the magnet bore. T_2-weighted coronal and transverse images were acquired from twenty contiguous 1 mm thick slices through the mouse abdomen, using a rapid acquisition with refocused echoes (RARE) sequence with 4 averages of 128 phase encoding steps over a 3x3 cm field of view, an echo time (TE) of 36 ms, a repetition time (TR) of 4.5 s and a RARE factor of 8. The resolution was 0.234 x 0.234 mm/pixel and the acquisition time was 3 minutes 24 seconds. Volumetric data was analysed using in-house software (ImageView) (16).

Immunoblot analysis

Total protein was extracted from equal size tumor pieces in SDS sample buffer using Precellys24. The following antibodies were used to detect protein levels (all from Cell Signaling): phospho-p53 (9284), cleaved caspase 3 (9661), caspase 3 (9665), p-ATM (5883p), phospho-ATR (2853p), phospho-CHK2 (2661p), GAPDH (8884s), γ-H2AX (9718x), and tubulin (2128L). Also used were antibodies against p19ARF (Novus Biologicals, 5-c3-1), and horseradish peroxidase (HRP) conjugated-p53 (R&D system, HAF1355). Proteins were detected using

Author Manuscript Published OnlineFirst on March 29, 2016; DOI: 10.1158/0008-5472.CAN-15-1939
Author manuscripts have been peer reviewed and accepted for publication but have not yet been edited.

HRP-conjugated anti-mouse and anti-rabbit antibodies (Dako), ECL Ultra (TMA-6) (Lumigen) and imaged using a Fujifilm LAS-4000 system.

Immunohistochemistry

Tumors were processed using a ASP300S tissue processor (Leica) according to the manufacturer's instructions. Sections were deparaffinized and dehydrated through Histo-Clear and graded alcohol series, rinsed for 5 min in tap water, boiled for 5min in 1% citric buffer and left to cool to RT. Endogenous enzyme activity was blocked by 1% H_2O_2 for 20min followed by 3 washes in ddH_2O. For mouse antibodies we used the M.O.M kit (Vector BMK-2202), for rabbit, the following protocol was used; blocking for >1h in PBS 0.01% Triton, 5% BSA, 1st antibody was incubated at RT overnight 1:100-1:500, washed in TBS, 2nd Biotinylated Anti Rabbit was incubated at RT for >2h (1:500), 3rd avidin HRP conjugated (A2664) (1:1000) 1hr RT. Antibody solution; PBS 0.01% Triton, 1% BSA. Sections were stained for 1-5 min using Vector Imm PACT DAB (SK-4105). We used the following antibodies; CD31 (ab28364), cleaved caspase 3 (Cell Signaling 9661), neurofilament-L (NF-L) (Cell Signaling 2837), Tuj-1 (R&D systems, BAM1195). Sections were counter-stained with hematoxylin and eosin. Immunofluorescence staining was performed using Invitrogen Alexa Fluor 488 goat anti-rabbit. Images were captured by confocal microscopy (LSM700, LSM T-PMT) and processed by ZEN2012 (Zeiss) software.

Real-time PCR

Total RNA was isolated from tumor tissue using the miRNAeasy minikit (Qiagen) and cDNA prepared using Superscript II Reverse Transcriptase (Life Technologies). Quantitative PCR (QT-PCR) was performed in triplicate using Taqman Gene Expression mix (Life Technologies) and gene-specific primers for *Cdkn1a* (Mm04205640), *Puma* (Mm00519268), *Noxa-1* (Mm00549172), *Bax* (Mm00432051) and *Actb* (Mm00607939) (Life Technologies). Relative expression was calculated according to the ΔΔCt relative quantification method against the average expression of control tumors.

Hypoxia

Tumor hypoxia was assessed as previously described (16,17). Briefly, tumor-bearing mice received 60 mg/kg i.p. of the hypoxia marker pimonidazole hydrochloride (Hypoxyprobe). After 45 min, tumors were rapidly excised, snap-frozen and stored in liquid nitrogen. Sections were either stained using Hypoxyprobe-1 plus FITC-conjugated mouse monoclonal antibodies (1:100), or HRP conjugated rabbit anti-FITC (Hypoxyprobe-1 Plus Kit).

Author Manuscript Published OnlineFirst on March 29, 2016; DOI: 10.1158/0008-5472.CAN-15-1939
Author manuscripts have been peer reviewed and accepted for publication but have not yet been edited.

Quantitation of reactive oxygen species

Freshly excised tumor samples (~20mg) were incubated with 10μM CellROX Oxidative Stress, (Molecular probes, C10444) for 1hr. Subsequently single cells were washed twice with PBS and fixed with 4% PFA for 1h, washed in PBS and acquired by FACS (BD-LSRII) using FACSDiva software (BD Biosciences). Sample were analysed by FlowJo (FlowJo LLC).

Glutathione assay

Glutathione was measured in fresh tumor samples using the GSH-Glo glutathione assay (Promega). Luciferase levels were normalized to tissue mass.

Statistical Analysis

Sample were compared using one-way ANOVA or two way ANOVA as indicated and post-hoc Bonferroni multiple comparison tests using GraphPad Prism; p values < 0.05 were considered as statistically significant.

Author Manuscript Published OnlineFirst on March 29, 2016; DOI: 10.1158/0008-5472.CAN-15-1939
Author manuscripts have been peer reviewed and accepted for publication but have not yet been edited.

Results

Th-*MYCN* transgenic mice display a normal p53 response

During tumorigenesis the expression or activity of checkpoint regulators, including p53, are often suppressed. We sought to establish whether this is also the case in our GEM model of MYCN-driven neuroblastoma (Th-*MYCN)*. To this end we tested the levels of the p53 upstream regulator $p19^{Arf}$ in matched tumor and spleen tissues and found similar protein expression levels (Fig. S1A), suggesting that the p53 pathway is intact. We also examined p53 activation following stress by exposing Th-*MYCN* tumor-bearing mice to cytotoxic ionizing radiation (IR). The p53 pathway was induced by IR as evidenced by increased levels of transcriptionally active p53 phosphorylated at serine 15 ($p\text{-}p53^{Ser15}$) in tumors, spleen and thymus (Fig. S1B), as well as an increase in the p53 target gene *Cdkn1a* ($p21^{Cip1/Waf1}$) (Fig. S1C). Furthermore, we found tumor-specific upregulation of the pro-apoptotic gene *Bbc3* (*Puma*), but not the pro-apoptotic genes *Pmaip1* (*Noxa*) or *Bax* (Fig. S1C, D). Both the cyclin-dependent kinase inhibitor p21 and Puma are well-characterized effectors of p53-mediated growth arrest and apoptosis. Consistent with this, apoptosis was enhanced as evidenced by the presence of cleaved caspase3 (CC3) in the tumor and the thymus (Fig. S1B and S2). Induction of DNA damage was demonstrated by the presence of phosphorylated histone gamma-H2AX (γ-H2AX), primarily in the spleen and the gut (Fig. S2). Taken together, these results suggest that Th-*MYCN* mice are representative of p53 wild-type (WT) human neuroblastoma.

p53 loss-of-function leads to increased tumor penetrance in Th-*MYCN* hemizygous mice

In order to evaluate p53 loss-of function in neuroblastoma, we crossed Th-*MYCN* mice (in which expression of a human *MYCN* transgene is directed by a rat tyrosine hydrolase (Th) promoter to neural crest cells during early development) (14) with a GEM model conditionally deficient for functional p53 (Fig. 1A) (15). Here, the endogenous *Trp53* gene is replaced with a knock-in allele ($Trp53^{KI}$) encoding a 4-hydroxytamoxifen (4-OHT)-regulatable $p53ER^{TAM}$ fusion protein. In the presence of 4-OHT (a metabolite of tamoxifen, Tam), the hormone-binding domain of the estrogen receptor (ER) is released from its inhibitory conformation and $p53ER^{TAM}$ is translocated to the nucleus. Homozygous Th-*MYCN* transgenic mice display 100% penetrance (18), developing tumors within seven to eight weeks of birth, whereas only 16% of hemizygous Th-*MYCN* transgenic mice with wild-type (WT) *Trp53* (Th-*MYCN*/$Trp53^{WT/WT}$) developed tumors by 21 weeks of age with a median latency of 62 days (Fig. 1B, Table S1). Thus penetrance and latency in the Th-*MYCN* GEM model are dependent on transgene dosage and in this study only

Author Manuscript Published OnlineFirst on March 29, 2016; DOI: 10.1158/0008-5472.CAN-15-1939
Author manuscripts have been peer reviewed and accepted for publication but have not yet been edited.

heterozygous Th-MYCN mice were used. While Th-*MYCN* mice heterozygous for *MYCN* and *Trp53*^{KI} (Th-*MYCN*/*Trp*53$^{KI/WT}$) displayed a moderate increase in penetrance to 27% with no significant decrease in tumor-free survival, this increased dramatically to 75% for mice homozygous for *Trp53*^{KI} (Th-*MYCN*/*Trp*53$^{KI/KI}$). No littermates lacking Th-*MYCN*, either heterozygous or homozygous for *Trp53*^{KI}, developed neuroblastomas by 200 days. While *Trp53*^{KI} homozygosity increased penetrance, this had no effect on either latency or tumor growth rate as measured by volumetric magnetic resonance imaging (MRI) (Fig. 1C).

To test whether the increased tumor incidence in Th-*MYCN*/*Trp*53$^{KI/WT}$ mice was due to a mutation in the WT *Trp53* allele, we sequenced exons 5-9 (corresponding to the p53 DNA binding domain) in Th-*MYCN*/*Trp*53$^{WT/WT}$ (n = 16), Th-*MYCN*/*Trp*53$^{KI/WT}$ (n = 12) and Th-*MYCN*/*Trp*53$^{KI/KI}$ (n = 11) tumors. We found only one mutation arising in the Th-*MYCN*/*Trp*53$^{KI/WT}$ cohort (Table S2), supporting the notion that increased tumor penetrance in Th-*MYCN*/*Trp*53$^{KI/WT}$ mice is not caused by inactivation of the remaining WT *Trp53* allele. We also examined whether post-natal Tam-induced restoration of functional p53 could affect tumor penetrance, latency and growth rate. We administered Tam to tumor-bearing mice aged 50-80 days as well as to 30-day old mice, a timepoint at which tumors are not yet detectable. We found that restoration of functional p53ER^{TAM} had no effect on tumor growth rate or penetrance in Th-*MYCN*/*Trp*53$^{KI/KI}$ mice (Fig. S3 A, B).

Pathological investigations in Th-*MYCN*/*Trp*53^{KI} transgenic mice revealed that they developed paravertebral, thoracic or abdominal solid tumors, consistent with a parasympathetic origin in common with the Th-*MYCN* GEM model. Immunohistochemical analysis revealed that all Th-*MYCN*/*Trp*53^{KI} tumors stained positive for the neuroblastoma markers Tuj-1 and neurofilament-L (NF-L) (Fig. 1D). Furthermore, in agreement with the parasympathetic origin of the Th-*MYCN* tumors (19), histopathological analysis revealed an increase in the percentage of pups positive for neuroblast hyperplasia in the Th-*MYCN*/*Trp*53$^{KI/KI}$ compared to Th-*MYCN*/*Trp*53$^{WT/WT}$ (Fig. S4). Thus our results suggested that p53 loss-of-function interacts with aberrant expression of *MYCN* at an early stage of neuroblastoma tumorigenesis. However, p53 deficiency did not affect latency or tumor growth rate.

MYCN-driven neuroblastomas deficient for p53 are resistant to apoptosis induced by IR

Given that p53 pathway alterations are associated with relapsed/treatment-resistant neuroblastoma, we tested whether p53 deficiency conferred an anti-apoptotic advantage to tumors in Th-*MYCN*/*Trp*53$^{KI/KI}$ mice. External beam radiotherapy is widely used in neuroblastoma treatment following induction chemotherapy and surgery, although a period of remission is often followed by subsequent relapse in high-risk cases (20). To examine a role for p53 deficiency in treatment-resistant neuroblastoma, we exposed Th-*MYCN*/*Trp*53$^{WT/WT}$ and Th-*MYCN*/*Trp*53$^{KI/KI}$ tumor-bearing mice to IR in the presence or absence of tamoxifen. In Th-*MYCN*/*Trp*53$^{WT/WT}$ tumors, 5Gy IR induced apoptosis 5.5 hours post-IR as measured by the presence of pyknotic nuclei in 90-95% of the cells (Fig. 2A). By contrast, Th-*MYCN*/*Trp*53$^{KI/KI}$ tumors were found to be resistant to IR-induced apoptosis. This resistance was maintained in some individual animals upon Tam-induced restoration of functional p53ER^{TAM} with responses ranging from IR resistance to complete response (Fig. 2A). IR also failed to significantly improve survival in Th-*MYCN*/*Trp*53$^{KI/K}$ allografts, providing evidence for intrinsic resistance to IR in these tumors (Fig. 2B). While the degree of activation of p53ER^{TAM} was similar (as measured by nuclear p-p53^{Ser15} and induction of *Cdkn1a* expression) post IR and Tam administration, this did not correlate with induction of apoptosis. Furthermore, tumors that showed a similar degree of p53 activation displayed differences in apoptotic response (Fig. 2C, D). Pharmacokinetic analysis (LC-MS/MS) of Tam levels supported these findings with results showing a significant correlation between levels of Tam and 4-OHT but no apoptotic response (Fig. 2E). Collectively these results suggest that p53 loss-of-function confers an anti-apoptotic advantage to tumors in response to cytotoxic IR, and that a fraction of Th-*MYCN*/*Trp*53$^{KI/KI}$ tumors develop resistance to restoration of p53 function.

p53 loss-of-function leads to upregulation of the GSH antioxidant metabolic pathway in MYCN-driven neuroblastoma

To characterize the mechanisms underlying resistance to IR in Th-*MYCN*/*Trp*53$^{KI/KI}$ tumors, we performed Affymetrix expression microarray analysis. Surprisingly, few genes (only 38 protein-coding transcripts) were altered across the Th-*MYCN*/*Trp*53$^{KI/KI}$ cohort of tumor samples compared with Th-*MYCN*/*Trp*53$^{WT/WT}$ tumors. This is may be due to a high degree of inter-tumoral heterogeneity in the pattern of gene expression among Th-*MYCN*/*Trp*53$^{KI/KI}$ tumors as revealed by hierarchical clustering (Fig. 3A) and principal component analysis (Fig. 3B). While Th-*MYCN*/*Trp*53$^{WT/WT}$ tumors cluster together tightly, this is not replicated in the Th-*MYCN*/*Trp*53$^{KI/KI}$ cohort. Thus, to identify pathways that may be altered in common among Th-*MYCN*/*Trp*53$^{KI/KI}$ tumors, we analysed gene expression in individual Th-*MYCN*/*Trp*53$^{KI/KI}$ tumors against the Th-*MYCN*/*Trp*53$^{WT/WT}$ control cohort. Differentially expressed genes were combined and analysis of the composite gene list revealed seven significantly altered pathways between the groups. (Table S3). Of these, we identified the glutathione metabolism pathway, which is associated with drug resistance (21-23), to be differentially regulated (Table S3). An

Author Manuscript Published OnlineFirst on March 29, 2016; DOI: 10.1158/0008-5472.CAN-15-1939
Author manuscripts have been peer reviewed and accepted for publication but have not yet been edited.

examination of genes encoding components of the glutathione metabolism pathway in individual tumors revealed upregulation in 50% of Th-*MYCN*/*Trp*53$^{KI/KI}$ tumors. Furthermore, the glutathione S-transferase (GST) family, including *GSTZ1* and *GSTP1*, represented the largest group (7 out of 17 genes) (Table 1). Glutathione and antioxidants have been shown to affect tumor initiation and drug resistance (23) and overexpression of *GSTP1* (24) and *GSTZ1* correlate with poor survival in neuroblastoma patients (Fig. 3C).

p53 deficiency leads to an increase in the GSH pool in response to chronic oxidative stress in MYCN-driven neuroblastoma

Glutathione S-transferase (GST) catalyzes the conjugation of the reduced form of glutathione (GSH) to xenobiotic substrates or unstable molecules such as hydrogen peroxide or other reactive oxygen species (ROS) for the purpose of detoxification (Fig. 3D). To examine whether the upregulation of GST is correlated with changes in the GSH redox cycle, we performed metabolic analysis using gas-chromatography mass spectrometry (GC-MS). We identified 12 metabolites that were significantly altered between Th-*MYCN*/*Trp*53$^{WT/WT}$ and Th-*MYCN*/*Trp*53$^{KI/KI}$ tumors (Table 2). Consistent with our gene expression data, the glutathione pool was increased by 3.7-fold in Th-*MYCN*/*Trp*53$^{KI/KI}$ tumors, together with a 4.3-fold decrease in glycine, a glutathione precursor (Table 2). The increase in GSH in Th-*MYCN*/*Trp*53$^{KI/KI}$ tumors was confirmed using the GSH-Glo glutathione assay (Fig. 3E). Interestingly, p53 restoration did not reverse this metabolic adaptation, with high GSH levels maintained in Th-*MYCN*/*Trp*53$^{KI/KI}$ tumors. Upregulation of the GSH antioxidant metabolic pathway in p53-deficient MYCN-driven neuroblastoma suggested an increased requirement for detoxification of GST substrates, such as derivatives of ROS that are implicated in tumorigenesis, disease progression and drug-induced resistance (25). Furthermore, c-MYC over-expression and p53 loss-of-function have previously been shown to be associated with an alteration in ROS levels (2,26-28). Consistent with these results, we found a significant increase in ROS-positive cells in Th-*MYCN*/*Trp*53$^{KI/KI}$ tumors (mean of 64%) compared with Th-*MYCN*/*Trp*53$^{WT/WT}$ tumors (mean of 14%) (Fig. 4A–C).

Furthermore, in agreement with the data shown in Fig. 2, restoration of p53ER^{TAM} activity reduced the percentage of ROS-positive cells in ~50% of tumors (Fig. 4C). This suggests that enhanced ROS levels may be regulated (either directly or indirectly) by p53 in a fraction of Th-*MYCN*/*Trp*53$^{KI/KI}$ tumors. As noted above, this was not associated with a decrease in tumor growth or improved overall survival (Fig. S3). Evidence for the presence of increased oxidative stress in Th-*MYCN*/*Trp*53$^{KI/KI}$ tumors was supported by the finding of enhanced staining for 8-hydroxyguanosine (8-OHdG), a modified base that occurs in DNA due to attack by hydroxyl

Author Manuscript Published OnlineFirst on March 29, 2016; DOI: 10.1158/0008-5472.CAN-15-1939
Author manuscripts have been peer reviewed and accepted for publication but have not yet been edited.

radicals (29). (Fig. 4D). ROS levels can also be increased by hypoxia and staining with the hypoxia marker pimonidazole, revealed that Th-*MYCN*/*Trp*53$^{KI/KI}$ tumors contained increased perinecrotic hypoxic regions (Fig. 4E, F). Increased ROS has been reported to lead to damage to enzymes, membranes and DNA (29,30) but despite enhanced 8-OHdG staining (Fig 4D), we found no significant changes in the levels of DNA damage markers (p-CHEK2 and γ-H2AX) between untreated Th-*MYCN*/*Trp*53$^{WT/WT}$ and Th-*MYCN*/*Trp*53$^{KI/KI}$ tumors (Fig. S5).

Our results suggest that resistance to IR in Th-*MYCN*/*Trp53*$^{KI/KI}$ mice may be due to metabolic adaption to chronic oxidative stress through up-regulation of GST pathway genes and increased levels antioxidant metabolites. This implied that the depletion of the GSH pool could resensitize IR-resistant p53 deficient neuroblastoma cells. Thus, we treated tumors with buthionine sulfoximine (BSO), an inhibitor of GSH synthesis that targets glutamate cysteine ligase (GCL), the first enzyme of the cellular GSH biosynthetic pathway (Fig. 3D). We implanted Th-*MYCN*/*Trp*53$^{KI/KI}$ primary tumor cells subcutaneously into 129X1/SvJ-Tg Th-MYCN negative mice. Consistent with our findings in the Th-*MYCN*/*Trp*53$^{KI/KI}$ GEM model of spontaneous neuroblastoma, 50% of the allografted tumors in which p53 activity was restored by the addition of Tam displayed resistance to IR and a higher Ki-67 proliferative index (Fig. 5A). However, importantly, this resistance was abolished in the presence of BSO (Fig. 5B, C).

Discussion

In this study we have demonstrated that p53 deficiency combines with aberrant expression of *MYCN* to drive neuroblast hyperplasia and increased neuroblastoma penetrance. Restoration of functional p53ER^{TAM} prior to tumors reaching detectable size or during later stages failed to alter tumor growth or penetrance. These findings suggest that p53 has an important role in the early stages of neuroblastoma tumorigenesis in Th-*MYCN* transgenic mice. Furthermore, p53 loss-of-function gives rise to tumors that can acquire growth and survival mechanisms that are resistant to the reintroduction of functional p53. This is in stark contrast to a medulloblastoma GEM model driven by expression of MYCN and p53 deficiency, GTML/*Trp53*$^{KI/KI}$ (GTML; *Glt1–tTA/TRE–MYCN–Luc*), where restoration of functional p53ER^{TAM} by Tam led to increased survival and inhibition of tumor growth (5). Other transgenic models of p53 loss-of-function do, however, develop tumors that display partial resistance to the restoration of functional p53ER^{TAM} including lymphoma where a requirement for induction of the oncogenic signaling sensor p19^{ARF} was identified (31). Additionally, p53 restoration in K-Ras induced NSCLC failed to induce tumor regression but diminished the proportion of high-grade tumors (32).

Recent results have suggested that the outcome of p53 restoration in established tumors is highly context-dependent. There is now evidence that the tumor suppressor function of p53 may be due to maintenance of genomic stability as well as metabolic and oxidative balance rather than simply its canonical role as a transcriptional activator of cell-cycle inhibitory and pro-apoptotic effectors such as p21, PUMA, and NOXA (1,3). Consistent with these findings, we found that tumors with p53 loss-of-function displayed elevated ROS. Three characteristics of Th-MYCN/Trp53$^{KI/KI}$ tumors could contribute to the increased levels of ROS: MYCN expression, hypoxia, and p53 loss-of-function. MYCN-dependent metabolic adaptation has been shown to result in upregulation of glycolytic metabolism, which is associated with increase in ROS production (7,33). Hypoxia, on the other hand, can generate ROS via mitochondrial complex III (34) and p53 has been shown to regulate ROS and, in turn, to be regulated by ROS in a context-dependent manner (35). The low level of ROS in Th-MYCN/ *Trp*53$^{WT/WT}$ compared with Th-*MYCN*/*Trp*53$^{KI/KI}$ tumors suggests that MYCN alone cannot be the only driver and that loss of p53 is also required. A number of direct p53 targets involved in the antioxidant pathway have been identified such as MnSOD, sestrins (Sesn1-3), NRF2, ALDH4 (aldehyde dehydrogenase 4), GLS2 (glutaminase 2), TIGAR, and tumor protein p53-inducible nuclear protein 1

(TP53INP1) (2,36). However, p53 also has a context-dependent pro-oxidant function and can transcriptional upregulate genes with strong pro-oxidant properties including PIG1–13 (p53-inducible genes 1–13) (37). The dual pro-oxidant and anti-oxidant roles of p53 suggest a delicate interplay between p53 and ROS in normal cells and in the absence of p53 one might expect to see the changes in the ROS-redox equilibrium identified in this study. Thus the combination of MYCN expression, p53 loss-of-function and hypoxia leading to elevated ROS in Th-*MYCN*/*Trp*53$^{KI/KI}$ tumors may account for the resistance to cell death in the absence of functional p53ER^{TAM}. However the lack of cell death upon restoration of functional p53ER^{TAM} indicates that other mechanisms arose to compensate for the increased oxidative stress.

There are several reducing mechanisms that regulate ROS-driven oxidative stress by transferring an unstable electron to a stable molecule. Among them is the glutathione pathway, where glutathione peroxidase reduces hydrogen peroxide to water while it oxidizes GSH to form dithiol (GSSH). Several genes from the GSH pathway are regulated by p53, which can down-regulate glutathione peroxidase 1 (GPX1) and glutaredoxin 3 (GRX3) to reduce ROS (38,39). A compensatory increase in the GSH pathway in the absence of functional p53 is supported by our results with Th-*MYCN*/*Trp*53$^{KI/KI}$ tumors exhibiting significant changes in the glutathione pathway, further confirmed by an increase in the GSH pool as measured by multiple assays. In addition to the direct detoxification of hydrogen peroxide by GSH, GSH can also be conjugated to xenobiotic substrates for the purpose of detoxification of the metabolites produced within the cell by oxidative stress. This reaction is catalyzed by GST. Interestingly, we found that 7/12 of the altered genes in glutathione metabolism pathway are from the GST family. Up-regulation of GSTs is associated with chemo-resistance and appears to represent an adaptive response to increased cellular damage and an important protective mechanism (33,35,40). This role of GST is consistent with the resistance to IR exhibited by Th-*MYCN*/*Trp*53$^{KI/KI}$ tumors, even after restoration of functional p53ER^{TAM}. GSTP1 is transcriptionally regulated by MYCN (24) and, alongside GSTZ1, high expression of these genes are linked with poor outcome in neuroblastoma (http://r2.amc.nl). Consistent with this, high levels of GSH are associated with resistance to chemotherapeutic and targeted therapies, including those used in frontline treatment of neuroblastoma such as cyclophosphamide, as well as relapsed disease such as irinotecan and temozolomide (41-44).

The continuing high relapse rate and poor survival for high-risk neuroblastoma patients makes the development of new therapeutic approaches an urgent priority. While direct mutations to p53 are a rare event in *de novo* cases of neuroblastoma (6), examination of the

Author Manuscript Published OnlineFirst on March 29, 2016; DOI: 10.1158/0008-5472.CAN-15-1939
Author manuscripts have been peer reviewed and accepted for publication but have not yet been edited.

p53 pathway has underlined its role in the pathogenesis of high-risk neuroblastoma (45-50). The role of p53 loss-of-function in the pathogenesis of untreated neuroblastomas has thus far not been elucidated. Our study, however, strongly suggests that p53 plays an important role in the maintenance of redox homoeostasis. Thus in the absence of p53 tumors may metabolically adapt to acquire pro-survival characteristics that nullify the canonical pro-apoptotic effects of p53. We therefore suggest that strategies to target neuroblastomas with defective p53 function using reactivation of p53 through inhibition of the MDM2/p53 interaction would not be successful in a proportion of cases. Here, pharmacologic depletion of the GSH pool together with reactivation of p53 represents an alternative strategy. Furthermore, high GSH pool levels or elevated expression of *GSTP1*, *GSTZ1* or other glutathione pathway genes could serve as biomarkers for the stratification patients. In this study we used BSO, an inhibitor of GCL, to deplete the GSH pool but specific inhibitors of GSTP1 such as 8-methoxypsoralen are currently under development (51). The use of agents to deplete the GSH pool in combination with conventional therapeutics or molecularly-targeted drugs thus warrants further study in high-risk neuroblastoma.

Grant Support

This study was supported by grants from The Neuroblastoma Society (O.Y. and K.B.), The Felix White Cancer Charity (A.H.), Cancer Research UK and EPSRC to the Cancer Imaging Centre at ICR and RMH, in association with the MRC and Department of Health (England) (C1060/A10334 & C1060/A16464), The Wellcome Trust (091763Z/10/Z), an EPSRC Platform Grant (EP/H046526/1), NHS funding to the NIHR Biomedical Research Centre at The Royal Marsden and the ICR, and a Paul O'Gorman Postdoctoral Fellowship funded by Children with Cancer UK (Y.J.).

Acknowledgments

The authors wish to thank Alan Mackay, Pawan Poudel and Anguraj Sadanandam for valuable advice on bioinformatic analysis, Elizabeth Want and Volker Behrends for advice on mass-spectrometry analysis, and Hannah Webber, Laura M. Smith and Alexander Koers technical assistance with animal models. We would also like to thank Sue Eccles and Eitan Shaulian for critical reading of the manuscript.

References

1. Valente LJ, Gray DH, Michalak EM, Pinon-Hofbauer J, Egle A, Scott CL, et al. p53 efficiently suppresses tumor development in the complete absence of its cell-cycle inhibitory and proapoptotic effectors p21, Puma, and Noxa. Cell reports 2013;3(5):1339-45.
2. Puzio-Kuter AM. The Role of p53 in Metabolic Regulation. Genes & cancer 2011;2(4):385-91.
3. Vousden KH, Ryan KM. p53 and metabolism. Nature reviews Cancer 2009;9(10):691-700.
4. Berkers CR, Maddocks OD, Cheung EC, Mor I, Vousden KH. Metabolic regulation by p53 family members. Cell Metab 2013;18(5):617-33.
5. Hill RM, Kuijper S, Lindsey JC, Petrie K, Schwalbe EC, Barker K, et al. Combined MYC and P53 defects emerge at medulloblastoma relapse and define rapidly progressive, therapeutically targetable disease. Cancer cell 2015;27(1):72-84.
6. Pugh TJ, Morozova O, Attiyeh EF, Asgharzadeh S, Wei JS, Auclair D, et al. The genetic landscape of high-risk neuroblastoma. Nature genetics 2013;45(3):279-84.
7. Qing G, Li B, Vu A, Skuli N, Walton ZE, Liu X, et al. ATF4 regulates MYC-mediated neuroblastoma cell death upon glutamine deprivation. Cancer cell 2012;22(5):631-44.
8. Rapizzi E, Ercolino T, Fucci R, Zampetti B, Felici R, Guasti D, et al. Succinate dehydrogenase subunit B mutations modify human neuroblastoma cell metabolism and proliferation. Hormones & cancer 2014;5(3):174-84.
9. Das S, Bryan K, Buckley PG, Piskareva O, Bray IM, Foley N, et al. Modulation of neuroblastoma disease pathogenesis by an extensive network of epigenetically regulated microRNAs. Oncogene 2013;32(24):2927-36.
10. Wang C, Liu Z, Woo CW, Li Z, Wang L, Wei JS, et al. EZH2 Mediates epigenetic silencing of neuroblastoma suppressor genes CASZ1, CLU, RUNX3, and NGFR. Cancer research 2012;72(1):315-24.

11. Fukuoka H, Takahashi Y. The role of genetic and epigenetic changes in pituitary tumorigenesis. Neurologia medico-chirurgica 2014;54(12):943-57.
12. Workman P, Aboagye EO, Balkwill F, Balmain A, Bruder G, Chaplin DJ, et al. Guidelines for the welfare and use of animals in cancer research. Br J Cancer 2010;102(11):1555-77.
13. Kilkenny C, Browne WJ, Cuthill IC, Emerson M, Altman DG. Improving bioscience research reporting: the ARRIVE guidelines for reporting animal research. PLoS Biol 2010;8(6):e1000412.
14. Weiss WA, Aldape K, Mohapatra G, Feuerstein BG, Bishop JM. Targeted expression of MYCN causes neuroblastoma in transgenic mice. The EMBO journal 1997;16(11):2985-95.
15. Christophorou MA, Martin-Zanca D, Soucek L, Lawlor ER, Brown-Swigart L, Verschuren EW, et al. Temporal dissection of p53 function in vitro and in vivo. Nature genetics 2005;37(7):718-26.
16. Jamin Y, Tucker ER, Poon E, Popov S, Vaughan L, Boult JK, et al. Evaluation of clinically translatable MR imaging biomarkers of therapeutic response in the TH-MYCN transgenic mouse model of neuroblastoma. Radiology 2013;266(1):130-40.
17. Boult JK, Walker-Samuel S, Jamin Y, Leiper JM, Whitley GS, Robinson SP. Active site mutant dimethylarginine dimethylaminohydrolase 1 expression confers an intermediate tumour phenotype in C6 gliomas. The Journal of pathology 2011;225(3):344-52.
18. Rasmuson A, Segerstrom L, Nethander M, Finnman J, Elfman LH, Javanmardi N, et al. Tumor development, growth characteristics and spectrum of genetic aberrations in the TH-MYCN mouse model of neuroblastoma. PLoS One 2012;7(12):e51297.
19. Hansford LM, Thomas WD, Keating JM, Burkhart CA, Peaston AE, Norris MD, et al. Mechanisms of embryonal tumor initiation: distinct roles for MycN expression and MYCN amplification. Proceedings of the National Academy of Sciences of the United States of America 2004;101(34):12664-9.

20. Matthay KK, Villablanca JG, Seeger RC, Stram DO, Harris RE, Ramsay NK, et al. Treatment of high-risk neuroblastoma with intensive chemotherapy, radiotherapy, autologous bone marrow transplantation, and 13-cis-retinoic acid. Children's Cancer Group. N Engl J Med 1999;341(16):1165-73.
21. Townsend DM, Tew KD. The role of glutathione-S-transferase in anti-cancer drug resistance. Oncogene 2003;22(47):7369-75.
22. Tew KD. Glutathione-associated enzymes in anticancer drug resistance. Cancer research 1994;54(16):4313-20.
23. Traverso N, Ricciarelli R, Nitti M, Marengo B, Furfaro AL, Pronzato MA, et al. Role of glutathione in cancer progression and chemoresistance. Oxidative medicine and cellular longevity 2013;2013:972913.
24. Fletcher JI, Gherardi S, Murray J, Burkhart CA, Russell A, Valli E, et al. N-Myc regulates expression of the detoxifying enzyme glutathione transferase GSTP1, a marker of poor outcome in neuroblastoma. Cancer research 2012;72(4):845-53.
25. Sosa V, Moline T, Somoza R, Paciucci R, Kondoh H, ME LL. Oxidative stress and cancer: an overview. Ageing Res Rev 2013;12(1):376-90.
26. Graves JA, Metukuri M, Scott D, Rothermund K, Prochownik EV. Regulation of reactive oxygen species homeostasis by peroxiredoxins and c-Myc. The Journal of biological chemistry 2009;284(10):6520-9.
27. Ostrakhovitch EA, Cherian MG. Role of p53 and reactive oxygen species in apoptotic response to copper and zinc in epithelial breast cancer cells. Apoptosis : an international journal on programmed cell death 2005;10(1):111-21.
28. Vafa O, Wade M, Kern S, Beeche M, Pandita TK, Hampton GM, et al. c-Myc can induce DNA damage, increase reactive oxygen species, and mitigate p53 function: a mechanism for oncogene-induced genetic instability. Molecular cell 2002;9(5):1031-44.
29. Ziech D, Franco R, Pappa A, Panayiotidis MI. Reactive oxygen species (ROS)--induced genetic and epigenetic alterations in human carcinogenesis. Mutation research 2011;711(1-2):167-73.
30. Cooke MS, Evans MD, Dizdaroglu M, Lunec J. Oxidative DNA damage: mechanisms, mutation, and disease. FASEB journal : official publication of the

Author Manuscript Published OnlineFirst on March 29, 2016; DOI: 10.1158/0008-5472.CAN-15-1939
Author manuscripts have been peer reviewed and accepted for publication but have not yet been edited.

Federation of American Societies for Experimental Biology 2003;17(10):1195-214.

31. Martins CP, Brown-Swigart L, Evan GI. Modeling the therapeutic efficacy of p53 restoration in tumors. Cell 2006;127(7):1323-34.
32. Junttila MR, Karnezis AN, Garcia D, Madriles F, Kortlever RM, Rostker F, et al. Selective activation of p53-mediated tumour suppression in high-grade tumours. Nature 2010;468(7323):567-71.
33. Sabharwal SS, Schumacker PT. Mitochondrial ROS in cancer: initiators, amplifiers or an Achilles' heel? Nature reviews Cancer 2014;14(11):709-21.
34. Guzy RD, Hoyos B, Robin E, Chen H, Liu L, Mansfield KD, et al. Mitochondrial complex III is required for hypoxia-induced ROS production and cellular oxygen sensing. Cell Metab 2005;1(6):401-8.
35. Maillet A, Pervaiz S. Redox regulation of p53, redox effectors regulated by p53: a subtle balance. Antioxid Redox Signal 2012;16(11):1285-94.
36. Budanov AV. The role of tumor suppressor p53 in the antioxidant defense and metabolism. Subcell Biochem 2014;85:337-58.
37. Polyak K, Xia Y, Zweier JL, Kinzler KW, Vogelstein B. A model for p53-induced apoptosis. Nature 1997;389(6648):300-5.
38. Brynczka C, Labhart P, Merrick BA. NGF-mediated transcriptional targets of p53 in PC12 neuronal differentiation. BMC genomics 2007;8:139.
39. Tan M, Li S, Swaroop M, Guan K, Oberley LW, Sun Y. Transcriptional activation of the human glutathione peroxidase promoter by p53. The Journal of biological chemistry 1999;274(17):12061-6.
40. Waypa GB, Marks JD, Guzy R, Mungai PT, Schriewer J, Dokic D, et al. Hypoxia triggers subcellular compartmental redox signaling in vascular smooth muscle cells. Circulation research 2010;106(3):526-35.
41. Rocha CR, Garcia CC, Vieira DB, Quinet A, de Andrade-Lima LC, Munford V, et al. Glutathione depletion sensitizes cisplatin- and temozolomide-resistant glioma cells in vitro and in vivo. Cell Death Dis 2015;6:e1727.
42. Estrela JM, Ortega A, Obrador E. Glutathione in cancer biology and therapy. Crit Rev Clin Lab Sci 2006;43(2):143-81.

43. Montero AJ, Jassem J. Cellular redox pathways as a therapeutic target in the treatment of cancer. Drugs 2011;71(11):1385-96.

44. St-Coeur PD, Poitras JJ, Cuperlovic-Culf M, Touaibia M, Morin PJ. Investigating a signature of temozolomide resistance in GBM cell lines using metabolomics. J Neurooncol 2015;125(1):91-102.

45. Tweddle DA, Pearson AD, Haber M, Norris MD, Xue C, Flemming C, et al. The p53 pathway and its inactivation in neuroblastoma. Cancer Lett 2003;197(1-2):93-8.

46. Tweddle DA, Malcolm AJ, Cole M, Pearson AD, Lunec J. p53 cellular localization and function in neuroblastoma: evidence for defective G(1) arrest despite WAF1 induction in MYCN-amplified cells. Am J Pathol 2001;158(6):2067-77.

47. Kim E, Shohet J. Targeted molecular therapy for neuroblastoma: the ARF/MDM2/p53 axis. J Natl Cancer Inst 2009;101(22):1527-9.

48. Wolff A, Technau A, Ihling C, Technau-Ihling K, Erber R, Bosch FX, et al. Evidence that wild-type p53 in neuroblastoma cells is in a conformation refractory to integration into the transcriptional complex. Oncogene 2001;20(11):1307-17.

49. Gamble LD, Kees UR, Tweddle DA, Lunec J. MYCN sensitizes neuroblastoma to the MDM2-p53 antagonists Nutlin-3 and MI-63. Oncogene 2012;31(6):752-63.

50. Xue C, Haber M, Flemming C, Marshall GM, Lock RB, MacKenzie KL, et al. p53 determines multidrug sensitivity of childhood neuroblastoma. Cancer research 2007;67(21):10351-60.

51. de Oliveira DM, de Farias MT, Teles AL, Dos Santos Junior MC, de Cerqueira MD, Lima RM, et al. 8-Methoxypsoralen is a competitive inhibitor of glutathione S-transferase P1-1. Front Cell Neurosci 2014;8:308.

Author Manuscript Published OnlineFirst on March 29, 2016; DOI: 10.1158/0008-5472.CAN-15-1939
Author manuscripts have been peer reviewed and accepted for publication but have not yet been edited.

Table 1. Altered expression of genes in the glutathione pathway among individual Th-*MYCN*/*Trp*53$^{KI/KI}$ tumors versus Th-*MYCN*/*Trp*53$^{WT/WT}$ tumors.

Gene	Sample						
	82078	83997	84834	28914	69306	72224	26857
Gstm1	+						+
Gstm7	+						+
Gstm2							+
Gstm4	+						
Gstp1				+		+	+
Gstt1							+
Gstz							+
Mgst3	+						
Gstm3	+						+
Rrm2				+		+	
Anpep							
Gclc	+						
Gpx3	+			+		+	
Gstt2							+
Gstk1							+
Mgst1							+
Mgsta3							+

Table 2. Analysis of metabolites in p53 deficient tumors.

Metabolite	KIKI:WT/WT Ratio	p-value
Alanine	0.480	1.23E-02
Valine	0.496	3.26E-02
Threonine	0.544	3.90E-02
Glycine	0.233	2.38E-02
Succinate	0.631	4.47E-02
PEP	0.538	3.52E-02
Hypotaurine	0.382	4.50E-02
Hypoxanthine	1.924	2.81E-02
3-GP	0.531	4.33E-02
L-ascorbic acid	0.397	3.18E-02
Ribose-5-phosphate	0.651	3.13E-02
GSH pool	3.761	1.66E-02

Author Manuscript Published OnlineFirst on March 29, 2016; DOI: 10.1158/0008-5472.CAN-15-1939
Author manuscripts have been peer reviewed and accepted for publication but have not yet been edited.

Figure Legends

Figure1. p53 deficiency leads to increased tumor penetrance in MYCN-driven neuroblastoma.

A. Th-*MYCN* transgenic mice were crossed with a GEM model comprising a knock in of the *Trp53* allele ($Trp53^{KI}$) expressing tamoxifen-regulatable $p53ER^{TAM}$.

B. Kaplan-Meier survival curves for Th-*MYCN*/*Trp*$53^{WT/WT}$ (n = 101), Th-*MYCN*/*Trp*$53^{KI/WT}$ (n = 188; ns, p = 0.06) or Th-*MYCN*/*Trp*$53^{KI/KI}$ (n = 60; ****, p < 0.0001) transgenic mice as indicated. ****, p < 0.0001; log-rank test.

C. Tumor volume change (relative to day 0) determined by MRI at day 4 for Th-*MYCN*/*Trp*$53^{WT/WT}$ (n = 9) Th-*MYCN*/*Trp*$53^{KI/WT}$ (n = 7) and Th-*MYCN*/*Trp*$53^{KI/KI}$ mice (n = 8).

D. Representative images of tumor sections from Th-*MYCN*/*Trp*$53^{WT/WT}$, Th-*MYCN*/*Trp*$53^{KI/WT}$ and Th-*MYCN*/*Trp*$53^{KI/KI}$ tumors subjected to H&E and immunohistochemical staining for the marker of apoptosis cleaved caspase 3 (CC3), and neuroblastoma markers Tuj1 and NF-L (brown). Cell nuclei were counterstained with hematoxylin. Scale bar: 50μM.

Figure 2. Tumors deficient for p53 exhibit p53-dependent and independent treatment resistance.

A. Mice bearing 5mm palpable tumors were placed on normal or tamoxifen diet for 5 days followed by whole-body irradiation (IR, 5 Gy) or mock treatment. Irradiated Th-*MYCN*/*Trp53*$^{WT/WT}$ tumors treated (n = 6) or untreated (n = 4) with tamoxifen (Tam), and irradiated Th-*MYCN*/*Trp53*$^{KI/KI}$ tumors treated (n = 6) or untreated (n = 7) with Tam were analysed to quantify dead cells as indicated by H&E (left) and percentage values (right). Scale bar: 100 μM. *p = 0.03, unpaired t-test.

B. Tumor free survival analysis of Th-*MYCN*/*Trp*$53^{KI/KI}$ allografts from primary tissue, control (n = 8) and irradiated (n = 8).

C. Immunofluorescence analysis of phosphorylated $p53^{Ser15}$ (p-p53) of Th-*MYCN*/*Trp*$53^{KI/KI}$ irradiated Th-*MYCN*/*Trp53*$^{KI/KI}$ tumors treated (n = 6) or untreated (n = 7) with Tam. Lower panel shows cells nuclear counterstained with DAPI. Values for percentage nuclear phosphorylated $p53^{Ser15}$ and apoptotic cells are indicated and highlighted by a black border in 2A. Scale bar: 20 μM.

D. RT-PCR analysis of *Cdkn1a* expression relative to *Actb*. *Cdkn1a* expression was evaluated in Th-*MYCN*/*Trp*53$^{WT/WT}$ untreated tumors (n = 5) or tumors treated with IR (n = 6), as well as Th-*MYCN*/*Trp*53$^{KI/KI}$ untreated tumors (n = 5) or tumors treated with IR minus Tam (n = 5) or plus Tam (n = 4). ****p < 0.0001; *p = 0.04; unpaired t-test.

E. Correlation plot between the intratumoral concentrations of 4-OHT and tamoxifen expressed in nM (left, r = 0.86, n = 8, p < 0.01) and correlation plot between intratumoral concentrations of 4-OHT and percentage of dead cells (right, r = 0.01, n = 8, p = 0.97).

Figure 3. Transcriptomic analysis of p53 deficient tumors reveals upregulation of GSH antioxidant pathway genes and an increased GSH pool and purine metabolism

A-D. Affymetrix mouse transcriptome array analysis of Th-*MYCN*/*Trp*53$^{WT/WT}$ (n = 4) and Th-*MYCN*/*Trp*53$^{KI/KI}$ (n = 8) tumors.

A. Hierarchal clustering.

B. Principal component analysis of signal intensities.

C. Overall survival of human neuroblastoma patients according to low or high expression of GSTP1 and GSTZ1 (http://r2.amc.nl, Versteeg-88 database of human neuroblastoma samples, GEO Series GSE16476).

D. Schematic representation of the glutathione metabolic pathway.

E. Analysis of GSH using the GSH-Glo glutathione assay in samples from *MYCN*/*Trp*53$^{WT/WT}$ tumors (n = 4), untreated Th-*MYCN*/*Trp*53$^{KI/KI}$ tumors (n = 6), or Th-*MYCN*/*Trp*53$^{KI/KI}$ tumors treated with tamoxifen (Tam) (n = 4). *p = 0.02; unpaired t-test.

Error bars represent mean ± SD.

Figure 4. Th-*MYCN*/*Trp53*$^{KI/KI}$ tumors exhibit chronic oxidative stress.

A. Fluorescence staining for NF-L expression and the presence of reactive oxygen species (ROS) in Th-*MYCN*/*Trp*53$^{KI/KI}$ tumor cells. Scale bar: 50 μM.

B. Histogram of ROS intensity as stained by CellROX Green in Th-*MYCN*/*Trp*53$^{KI/KI}$, Th-*MYCN*/*Trp*53$^{WT/WT}$, or unstained negative control cells as indicated. Grey bar represents the intensity threshold for ROS positivity.

C. Flow cytometric analysis of ROS-positive cells in Th-*MYCN*/*Trp*53$^{WT/WT}$ tumors with (n = 7) or without (n = 9 tamoxifen or Th-*MYCN*/*Trp*53$^{KI/KI}$ tumors with (n = 6) or without (n = 4) tamoxifen. ****p < 0.0001; unpaired t-test.

Author Manuscript Published OnlineFirst on March 29, 2016; DOI: 10.1158/0008-5472.CAN-15-1939
Author manuscripts have been peer reviewed and accepted for publication but have not yet been edited.

D. Staining for the oxidative stress marker 8-hydroxyguanosine (8-OHdG) in Th-*MYCN*/*Trp*53$^{KI/KI}$ tumors. Scale bar: 100 μM.

E. Top, Fluorescence measurement of pimonidazole adduct formation in tumors from Th-*MYCN*/*Trp*53$^{WT/WT}$ (n = 7) or Th-*MYCN*/*Trp*53$^{KI/KI}$ (n = 7) mice. Data points represent the mean area for each individual tumor *p = 0.04; unpaired t-test. Bottom, representative fluorescence images from Th-*MYCN*/*Trp*53$^{WT/WT}$ and Th-*MYCN*/*Trp*53$^{KI/Ki}$ tumors as indicated.

F. H&E and immunohistochemical co-staining with CD31 and Hypoxyprobe in Th-*MYCN*/*Trp*53$^{WT/WT}$ and Th-*MYCN*/*Trp*53$^{KI/K}$ tumors. Scale bar: 100 μM.

Error bars represent mean ± SD.

Figure 5. Depletion of the GSH pool restores sensitivity to IR.

A-C. Mice bearing allografts derived from Th-*MYCN*/*Trp*53$^{KI/K}$ tumors were untreated (n = 4), treated with IR (n = 4), tamoxifen (Tam) (n = 4) or buthionine sulfoximine (BSO) (n = 4). Mice were injected bilaterally with tumor cells and 6-8 tumors analyzed per group. Scale bar: 50 μM.

A. H&E and immunohistochemical staining for cell proliferation (Ki-67) in Th-*MYCN*/*Trp*53$^{KI/KI}$ allografts responsive or resistant to treatment with IR and Tam as indicated.

B. Quantitative histopathological determination of cell death in Th-*MYCN*/*Trp*53$^{KI/KI}$ allografts treated with IR, Tam and/or BSO as indicated. *p = 0.03, unpaired t-test (one-tailed).

C. Total GSH levels in Th-*MYCN*/*Trp*53$^{KI/KI}$ allografts treated with IR and Tam, with or without BSO as indicated. *p = 0.04, unpaired t-test (one-tailed).

Error bars represent mean ± SD.

Figure 1

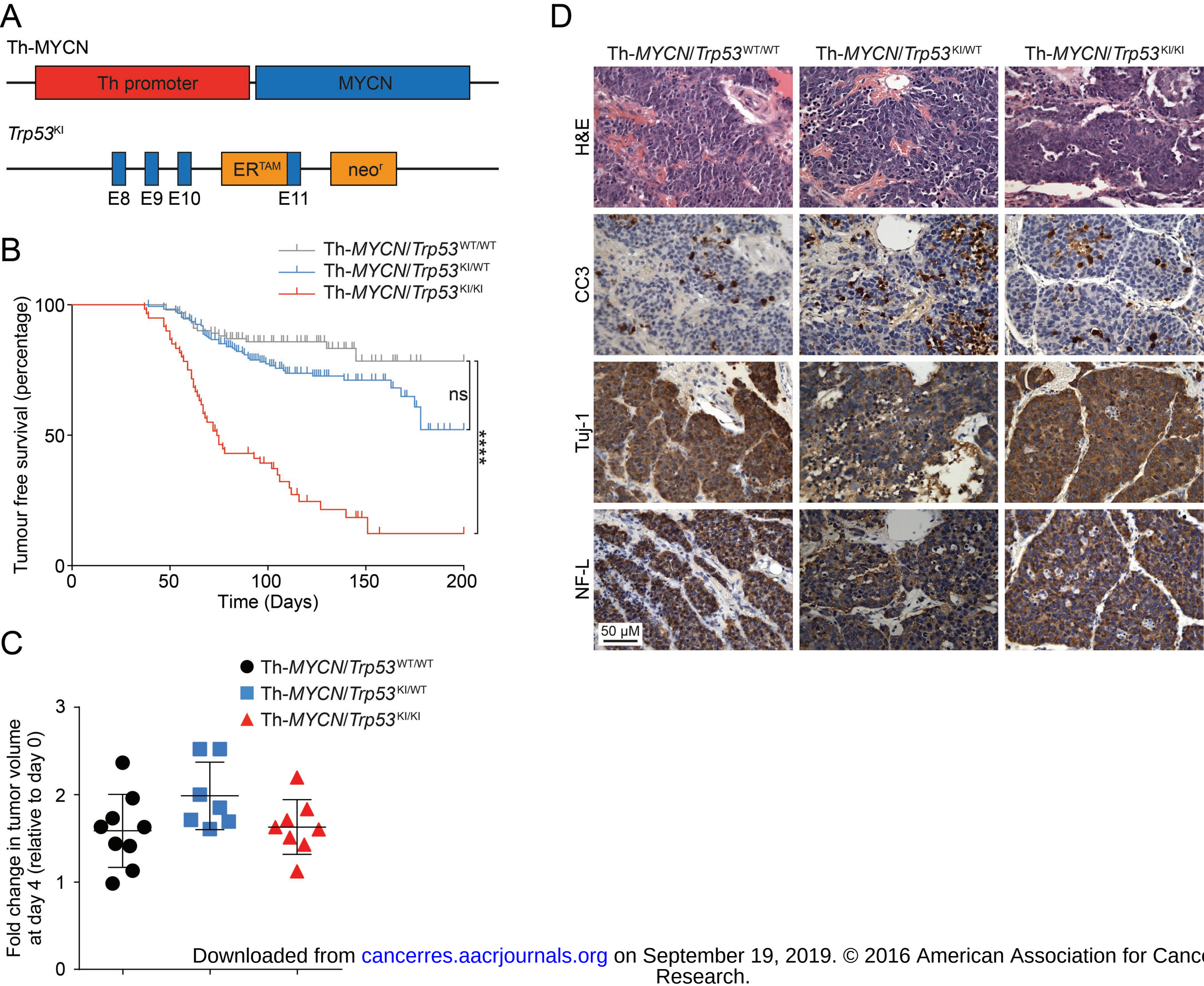
A
Th-MYCN
Th promoter
MYCN
Trp53KI
ERTAM
neor
E8 E9 E10 E11
B
Th-MYCN/Trp53WT/WT
Th-MYCN/Trp53KI/WT
Th-MYCN/Trp53KI/KI
Tumour free survival (percentage)
100
50
0
ns
****
0 50 100 150 200
Time (Days)
C
Th-MYCN/Trp53WT/WT
Th-MYCN/Trp53KI/WT
Th-MYCN/Trp53KI/KI
Fold change in tumor volume at day 4 (relative to day 0)
3
2
1
0
D
Th-MYCN/Trp53WT/WT
Th-MYCN/Trp53KI/WT
Th-MYCN/Trp53KI/KI
H&E
CC3
Tuj-1
NF-L
50 μM

Figure 2

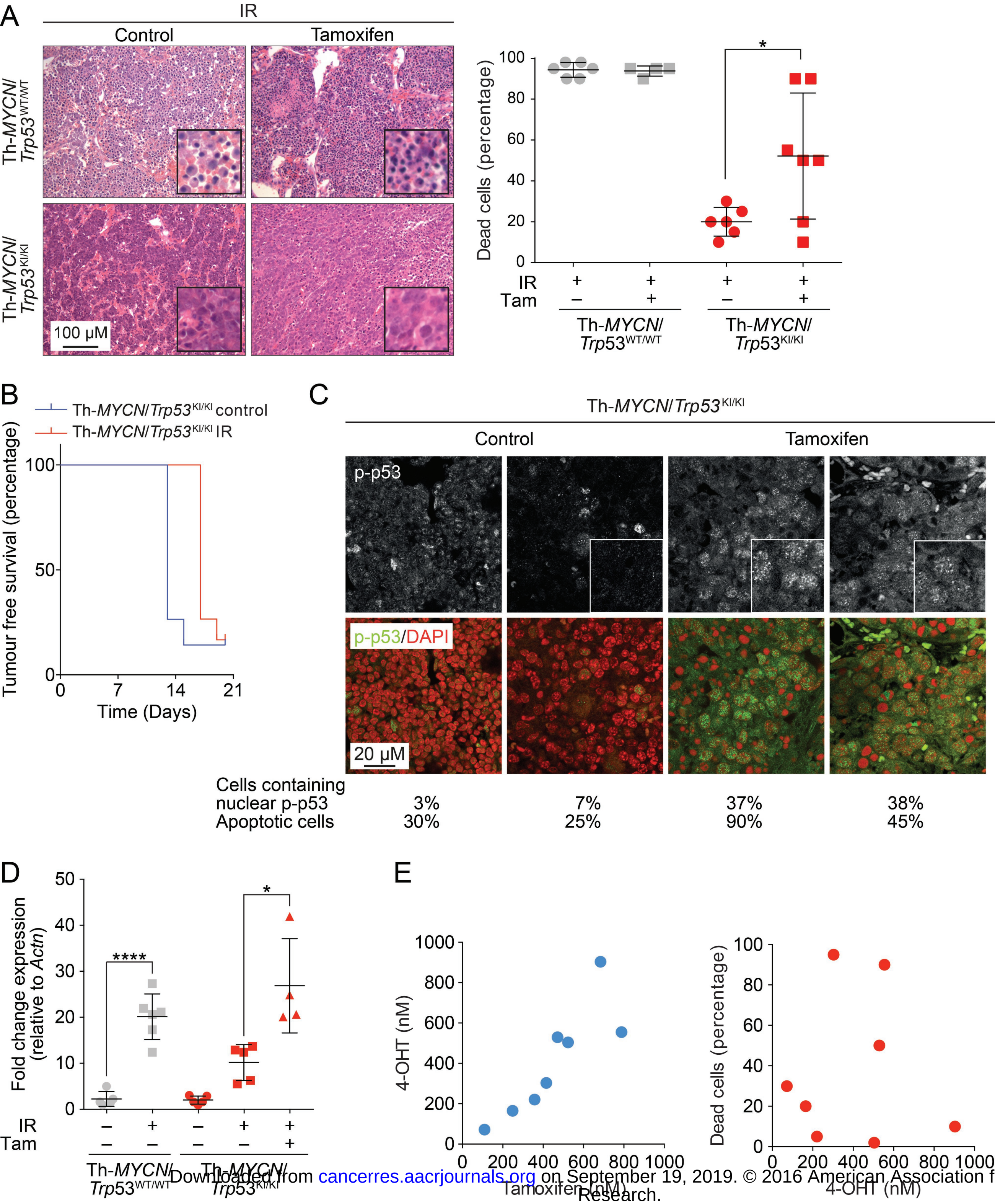

A
IR
Control
Tamoxifen
Th-MYCN/Trp53WT/WT
Th-MYCN/Trp53KI/KI
100 μM
Dead cells (percentage)
*
IR
Tam
B
Th-MYCN/Trp53KI/KI control
Th-MYCN/Trp53KI/KI IR
Tumour free survival (percentage)
Time (Days)
C
Th-MYCN/Trp53KI/KI
Control
Tamoxifen
p-p53
p-p53/DAPI
20 μM
Cells containing nuclear p-p53 3% 7% 37% 38%
Apoptotic cells 30% 25% 90% 45%
D
Fold change expression (relative to Actn)
****
*
IR
Tam
Th-MYCN/Trp53WT/WT
Th-MYCN/Trp53KI/KI
E
4-OHT (nM)
Tamoxifen (nM)
Dead cells (percentage)
4-OHT (nM)

Figure 3

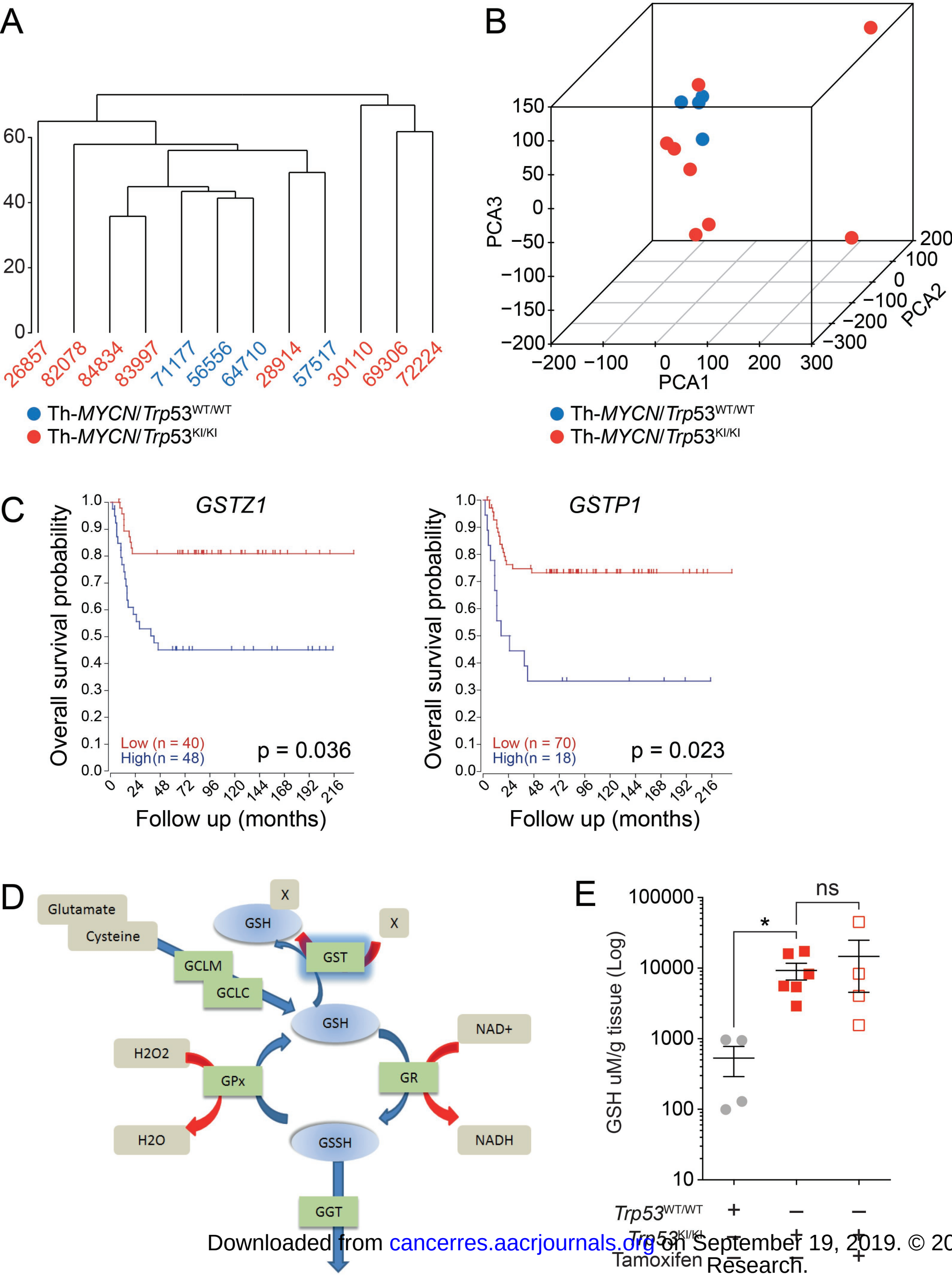
A
26857
82078
84834
83997
71177
56556
64710
28914
57517
30110
69306
72224
Th-MYCN/Trp53WT/WT
Th-MYCN/Trp53KI/KI
B
PCA1
PCA2
PCA3
C
GSTZ1
GSTP1
Overall survival probability
Follow up (months)
Low (n = 40)
High(n = 48)
p = 0.036
Low (n = 70)
High(n = 18)
p = 0.023
D
Glutamate
Cysteine
GCLM
GCLC
GSH
X
GST
GPx
GR
H2O2
H2O
NAD+
NADH
GSSH
GGT
E
GSH uM/g tissue (Log)
ns
*
Trp53WT/WT
Trp53KI/KI
Tamoxifen

Figure 4

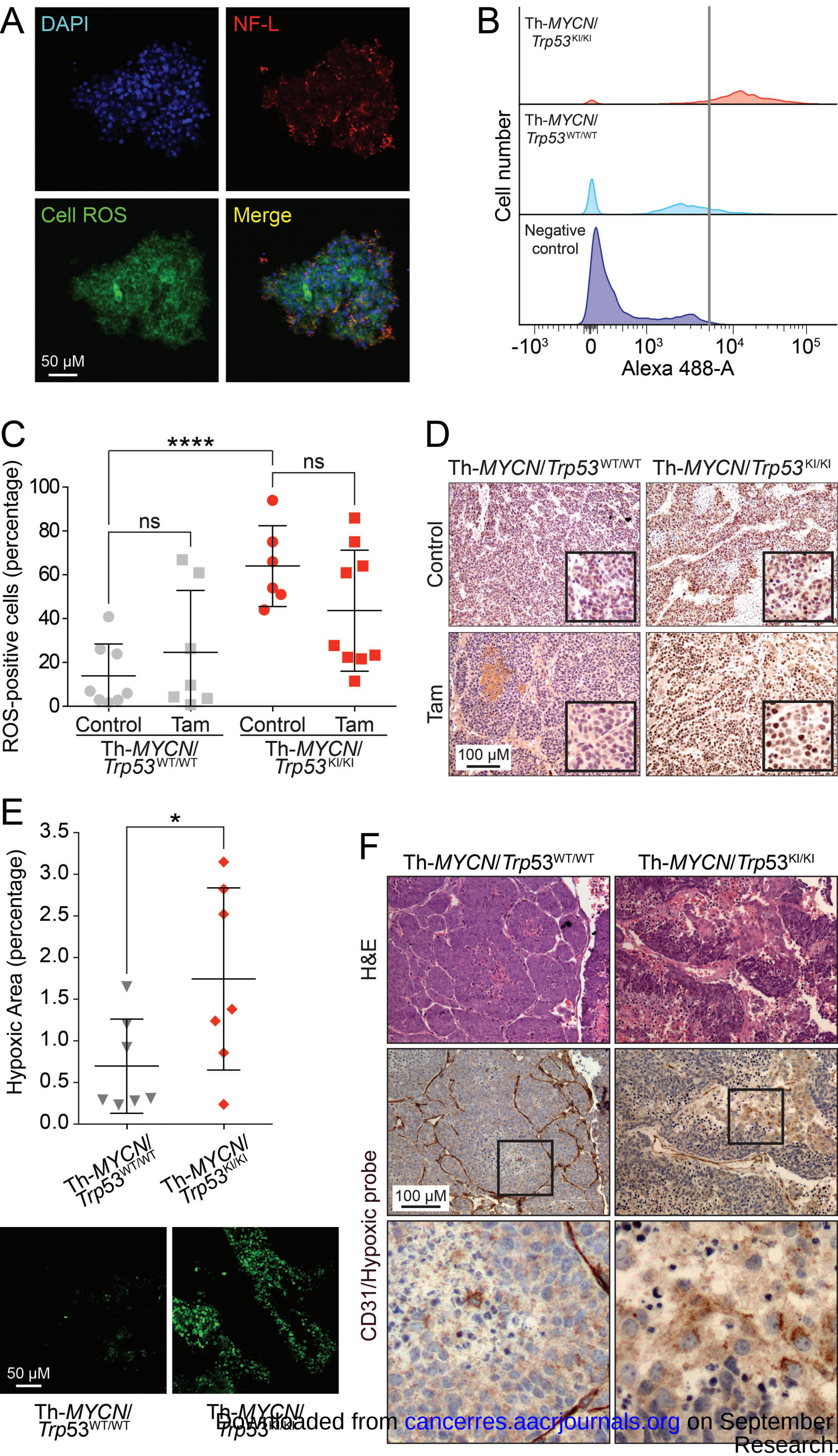

A
DAPI
NF-L
Cell ROS
Merge
50 μM
B
Th-MYCN/ Trp53KI/KI
Th-MYCN/ Trp53WT/WT
Negative control
Cell number
-10³
0
10³
10⁴
10⁵
Alexa 488-A
C
****
ns
ns
ROS-positive cells (percentage)
100
80
60
40
20
0
Control
Tam
Control
Tam
Th-MYCN/ Trp53WT/WT
Th-MYCN/ Trp53KI/KI
D
Th-MYCN/Trp53WT/WT
Th-MYCN/Trp53KI/KI
Control
Tam
100 μM
E
*
Hypoxic Area (percentage)
3.5
3.0
2.5
2.0
1.5
1.0
0.5
0.0
Th-MYCN/ Trp53WT/WT
Th-MYCN/ Trp53KI/KI
50 μM
Th-MYCN/ Trp53WT/WT
Th-MYCN/ Trp53KI/KI
F
Th-MYCN/Trp53WT/WT
Th-MYCN/Trp53KI/KI
H&E
CD31/Hypoxic probe
100 μM

Figure 5

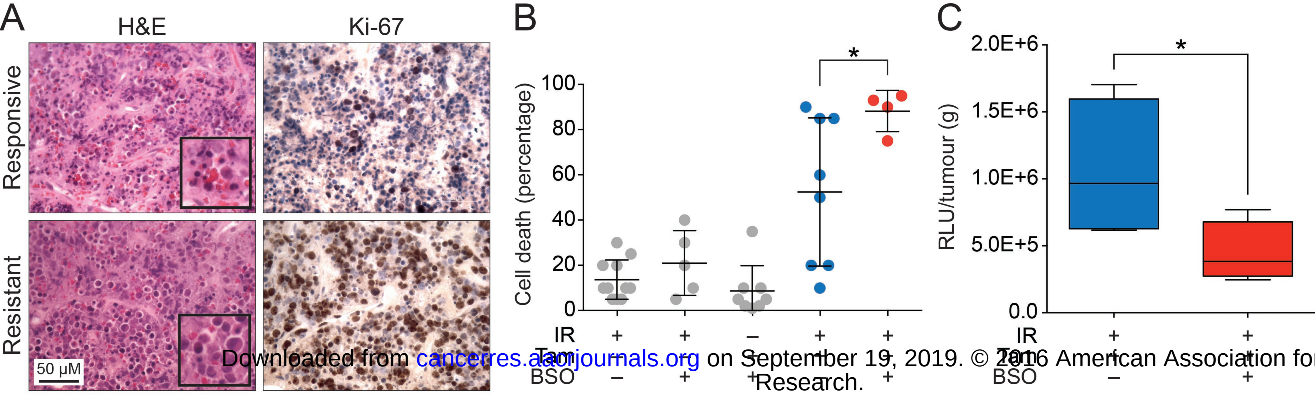
A
H&E
Ki-67
Responsive
Resistant
50 μM
B
*
Cell death (percentage)
100
80
60
40
20
0
IR + + – + +
Tam
BSO – + + – +
C
*
RLU/tumour (g)
2.0E+6
1.5E+6
1.0E+6
5.0E+5
0.0
IR + +
Tam
BSO – +

Cancer Research
The Journal of Cancer Research (1916–1930) | The American Journal of Cancer (1931–1940)

American Association for Cancer Research

p53 loss in Myc-driven neuroblastoma leads to metabolic adaptations supporting radioresistance

Orli Yogev, Karen Barker, Arti Sikka, et al.

Cancer Res Published OnlineFirst March 29, 2016.